

Surface-Slip Gradients of Large Earthquakes

by Bruce E. Shaw

Abstract For earthquakes that are large enough to break the earth's surface, slip can be measured directly, providing model-independent information of spatially varying behavior in earthquakes. Here new techniques are developed and applied to extract robust measures of surface slip. In particular, I examine how differences in slip scale with differences in separation. Examining slip distributions of seven large earthquakes in a digital database, I find that the curves collapse into a common behavior over kilometer to tens-of-kilometer length scales. Distributions of differences of slip are found to be reasonably well fit by normal distributions, with the variance of the distributions scaling with separation distance. In particular, average slip differences are seen to be increasing linearly out to length scales of the seismogenic crust, but with a nonzero intercept when extrapolated back to a zero separation of around 1 m offset. The variability of slip extrapolated to zero separation, the mean offset, of around 1 m ($.96 \pm .15$ m) is a remarkable feature of the observations, holding for all seven of the large earthquakes analyzed. Leaving aside the offset and looking at the increase as a function of separation, the slope or lateral strain has a value consistent with large scale average strains. Thus, behavior consistent with constant stress drop is seen at length scales smaller than the event size, revealing a further invariant of earthquake dynamics. Finally, taking into account the noisy environment by looking for coherent structures unlikely to be noise related, I find structures which have moderate values of lateral strains, on the order of a factor of 10 times mean values, with values appearing to be independent of length scale and magnitude.

Introduction

The deep depths where earthquakes initiate and the short unforeseen times over which they occur leave much of the information we have about them remote and underdetermined. In the case of large earthquakes which break the surface, however, geological observations of offsets across faults provide direct measurements of surface slip that are independent of any modeling assumptions. As such, these slip measurements provide a particularly valuable view of earthquake behaviors. Geologists have long recognized the importance of these measurements, and have expended great effort in collecting the data using a variety of markers. The collected surface-slip data have been used in a number of ways. Most commonly, it is used to anchor our views of individual events, providing ground truth against which geodetic and seismological measurements are compared. Average properties of surface slip have also been used to look at scaling laws (Scholz, 1982; Romanowicz, 1992, 1994; Scholz, 1994; Wells and Coppersmith, 1994; Bodin and Brune, 1996; Shaw and Scholz, 2001; Manighetti *et al.*, 2007; Wesnousky, 2008) and to find mean profiles of slip (Biasi and Weldon, 2006) and to categorize shapes of slip (Manighetti *et al.*, 2005; Wesnousky, 2008). Properties of the distributions of surface-slip values averaging over position along-strike have also been

measured for use in paleoseismic inferences of event magnitudes (Hemphill-Haley and Weldon, 1999).

Here, I take a new approach, examining statistical properties of the fluctuations in surface slip to try to extract useful information about earthquake ruptures. This approach is made difficult by large variability in individual surface-slip measurements along-strike. There are many potential factors contributing to the variability of slip along-strike; which factor or factors are most important remains an open question. Inelastic surface deformation in unconsolidated surface materials, secondary strands which distribute slip onto multiple surfaces, nonplanar geometry leading to mixed-mode variable oblique slip, and measurement uncertainties are some of the potential factors. Different surface conditions, such as water table and sedimentary consolidation and depths, may lead to different relative contributions of each of these factors. The analysis will not be able to disentangle what factors are ultimately contributing to the observed variability. It will, however, give a much better handle on what the variability is, an outcome that could aid future efforts in pinning down the sources of variability, and a result which is taken advantage of here to find further underlying systematics in the data.

This paper focuses on one measure of surface slip, the difference in surface slip as a function of distance between points. This quantity has a number of advantages. First, it is not sensitive to incompleteness in the observations: it can be made even when only some parts of a fault have measured offsets. Second, it has dimensions of strain and thus directly maps onto quantities of physical significance and interest. Third, because average stress drops, or similarly, strain drops, have been observed to be scale invariant across the whole range of earthquake sizes (Aki, 1972; Hanks, 1977; Shaw, 2009), one may expect that statistical measures of smaller scale features of this quantity may be of further significance. Finally, because the statistics of pairs of points are examined, a large ensemble is obtained when the number of slip measurements N is large, with the number of pairs scaling as $N^2/2$.

Data and Analysis

Extracting strain by differencing slip just at neighboring points gives hugely variable results and is not robust to noise. Slip can differ by substantial amounts at closely spaced points at the surface by meters of slip over even separations of tens of meters in extremely well-controlled settings (Rockwell *et al.*, 2002). With such large differences in slip, inferred strains are then more a function of separation of measurement locations than slip differences. Moreover, such large strains would shatter rocks, so they must be accommodated in unconsolidated materials in the near surface. How does one then see through these shallow layers and these apparently noisy measurements? Here, the power of statistical measures enables the extraction of a signal. By looking at how populations of slip differences change as separation changes, we can see through these noisy signals to find underlying trends.

To quantify slip gradients, I look at differences in slip S as a function of separation $|\vec{r}_i - \vec{r}_j|$ along the fault where \vec{r}_i and \vec{r}_j are two different positions along the fault rupture. The interest is in average behavior:

$$\langle |S(\vec{r}_i) - S(\vec{r}_j)| \rangle_{i>j} = f(|\vec{r}_i - \vec{r}_j|), \quad (1)$$

and also distributions of the values as a function of separation. At constant strain, these distributions should grow linearly with separation. What do the earthquake data show?

The slip data I use come from data compiled by Wesnousky (2008) and included in the electronic supplement to that paper. This data set is further restricted by considering only events with magnitude 7 or larger that occurred in the last 50 yr and that had at least 40 measured surface-slip values. This restriction leaves seven events: surface slips that are shown in Figure 1. Slip values in the database do not come with uncertainties. A strength of the analysis developed is that it will enable the derivation of effective uncertainties from the data. I perform the following analysis on the data. I form differences in slip and distance between all pairs of

points. To look for invariant features, attention is focused on length scales smaller than the event scale, focusing in particular on the separations of 20 km or less, to represent lengths equal to and smaller than the seismogenic crust.

Next, robust statistical measures of this ensemble are sought. I begin by using rank ordering to group points to avoid introducing intrinsic scales into the problem. Pairwise separation distances between point measurements are taken $r_{ij} = |\vec{r}_i - \vec{r}_j|$ for $i > j$ and rank ordered, from the closest to furthest distance. Then, going from the closest separation pairs to the farthest, the data are divided into nonoverlapping subsets of n points each. Rank ordering of each subset of n points ordered from the smallest difference in slip to the largest difference in slip is then done.

Figure 2 illustrates this rank ordering procedure, in darkening shades by groups and, here, using $n = 128$. In this figure, the bottom half of each group is shown in the lightest shade, the next quarter is shown in a darker shade, the next eighth is shown in yet a darker shade, the next sixteenth is shown in an even darker shade, and the rest are shown in the darkest shade. One significant feature of the data is that for the larger groups above the median, the shades above the lightest shade, when extrapolating back to a separation $r = 0$, one sees that the data have a nonzero slip difference. On reflection, this is not too surprising given that there are measurement errors and uncertainties in the individual data points. Some of this uncertainty is measurement uncertainty, some of this is other physical factors. I will not be able to separate out the different uncertainties here, but rather seek to quantify the variability and extract a signal which is not swamped by it.

Rank ordering makes clear that slip differences increase with increasing separation for almost all of the curves, as indicated by the upward trend of the rank-ordered groups. To quantify the dependence as a function of separation, the points are grouped into linear width bins. Points between separations r and $r + dr$ (width $dr = 2$ km here) are grouped, and the average values are plotted as a function of the middle of the bin separations. The average properties can be measured without assuming anything about the underlying distributions. Figure 3a shows the average difference in slip as a function of separation for all the events. Figure 3b shows the standard deviation as a function of separation. They are obviously closely related, so Figure 3c shows the ratios of the average to the standard deviation. On the same plot, a thin dashed black line shows the ratio of these two quantities for a normal distribution, which is $\sqrt{2/\pi} \approx .797$. For comparison, tick marks are also shown for an exponential distribution, which has a heavier tail (relatively more extreme values) than a normal distribution (and has an average to standard deviation ratio of $1/\sqrt{2} \approx .707$), and for a boxcar function (flat out to a maximum value, then zero after that), which has a minimal tail (and has an average to standard deviation ratio of $\sqrt{3}/2 \approx .866$). The normal distribution value is unambiguously a much better fit. The good fit of the normal distribution value to the average behavior

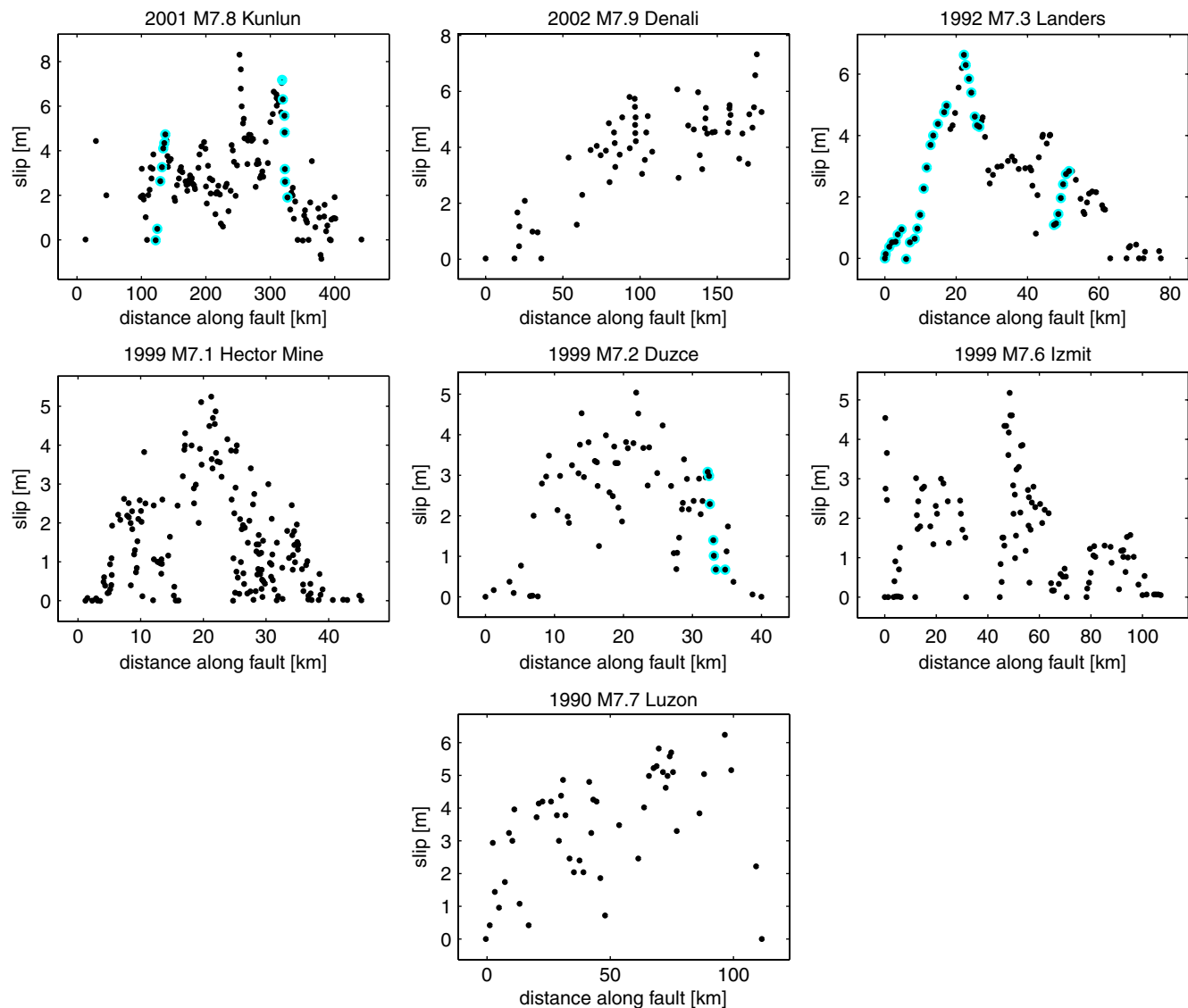


Figure 1. Surface slip data for large $M > 7$ earthquakes, from data compiled by Wesnousky (2008; see the Data and Resources section). All $M > 7$ events in the data set occurring in the last half century with $N > 40$ data points are shown and used in the following analysis. Points outlined in a lighter shade highlight coherent structures of a long stretch of sequentially increasing or sequentially decreasing slip, a subject discussed later in the paper. Original sources for the earthquakes shown here are as follows: 2001 M 7.8 Kunlun (Lin *et al.* 2002; Xu *et al.*, 2002; Klinger *et al.*, 2005, 2006); 2002 M 7.9 Denali (Haeussler *et al.*, 2004); 1992 M 7.3 Landers (Sieh *et al.* 1993); 1999 M 7.1 Hector Mine (Treiman *et al.*, 2002); 1999 M 7.2 Duzce (Akyuz *et al.*, 2002); 1999 M 7.6 Izmit (Barka *et al.* 2002); 1990 M 7.7 Luzon (Nakata, 1990; Yomogida and Nakata, 1994). The color version of this figure is available only in the electronic edition.

raises the question of what the underlying distributions are, a question which will be returned to shortly. But for now, let us continue our examination of these average behaviors, looking for systematics in them.

There are a number of interesting things to say about Figure 3. First, and very significantly, there is quite a good collapse of the data, with all of the curves being remarkably close to one another, certainly within a factor of 2. Second, there is an approximately linear trend in the difference in slip with increasing separation. Third, this linear trend has a non-zero offset, with a value of around 1 m when extrapolated back to zero separation. Not taking this offset into account would

wreak havoc on interpretations of strain at small distances, giving strain diverging as the inverse of the separation for constant difference in slip. A number of factors go into creating this offset, and I will not be able to disentangle them here. Nevertheless, the near constant offset value of around 1 m for all events is remarkable. There are a number of possible sources of this uncertainty; again, resolving which ones might be relevant are beyond the scope of this work. One possibility is intrinsic uncertainties in the slip measurements. Klinger *et al.* (2005) give an error estimate of 1 m in the optical imaging technique used in their measurements of the Kunlun earthquake, which forms a basis of the data for that earthquake

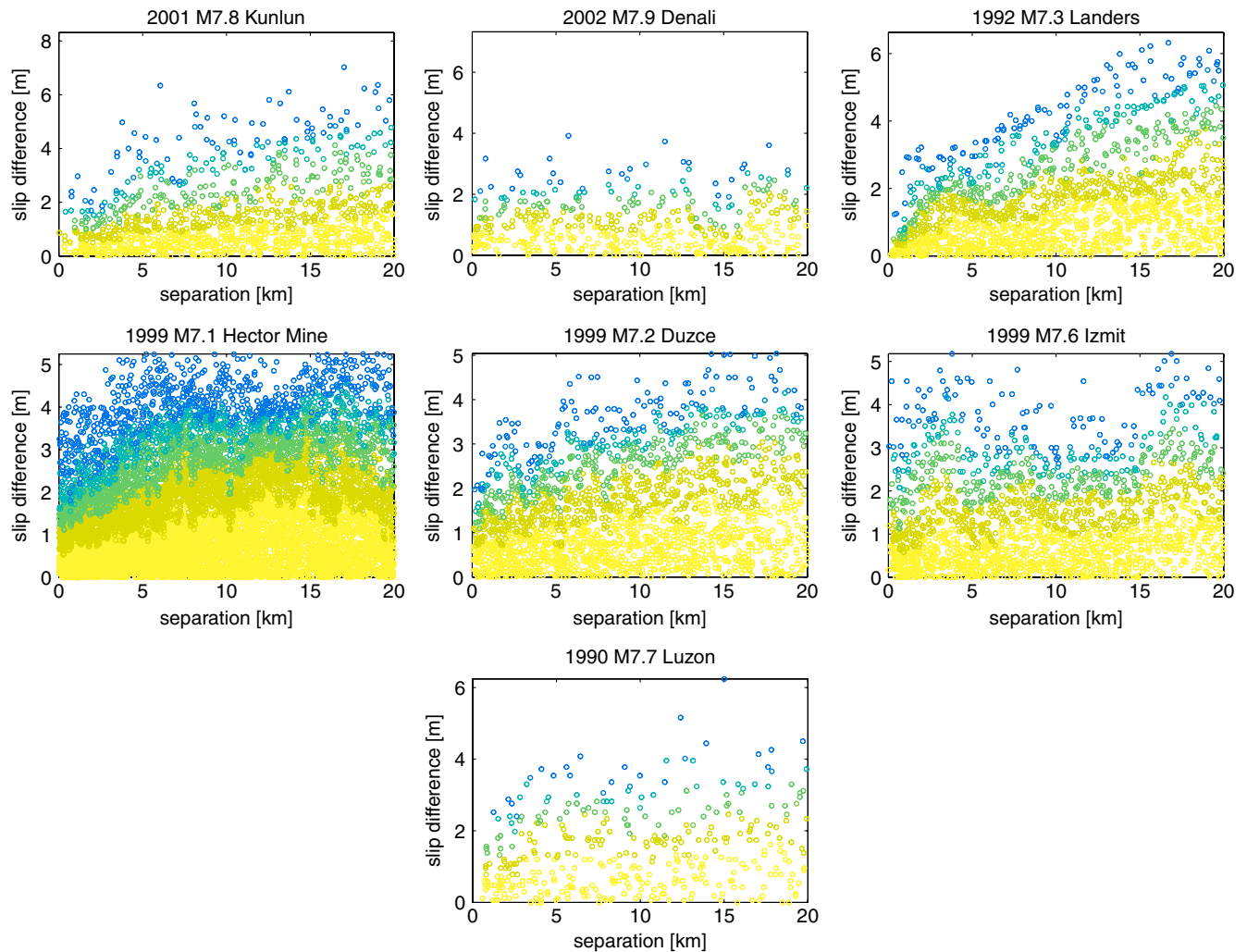


Figure 2. Differences of slip for all pairs of points separated by a distance less than 20 km. Differences in slip appear in darkening shades by rank order groups, as discussed in the [Data Analysis](#) section, with darker shades as higher ranking differences. The color version of this figure is available only in the electronic edition.

in the [Wesnousky \(2008\)](#) data set (see [Data and Resources](#) section). Another possibility is something physical. Nonplanar geometry effects would be an example of this. Another possibility might perhaps be measurement biases, whereby, during allocation of finite and precious fieldwork time, values where slip has changed sufficiently are given higher priority than values where slip has not changed. Again, there is not enough information here to disentangle the wide range of possibilities, and so I will continue by working around it.

Figure 4 shows the results of linear fits to the average slip difference curves in Figure 3a, showing offsets in Figure 4a and slopes in Figure 4b. The offsets give quite surprisingly stable values of around 1 m ($.96 \pm .15$ m mean value after correcting for bin width). The slopes are substantially noisier though, with deviations of a factor of 2 on either side of the mean ($.48 \pm .25 \times 10^{-4}$). The Denali event also seems to have a noticeably smaller slope than the other events. Given the noise and sparse data and limited magnitude range, it is difficult to say anything about any trends in

the data. The mean value of the slopes, $.5 \times 10^{-4}$, however, is quite interesting, being comparable to those mean values implied by constant stress drop and thus constant strain drop scaling for average large-scale behavior. That is, for stress drops of 3 MPa seen for small and large events, dividing by typical rock modulus values gives strain drops of $3 \text{ MPa}/30 \text{ GPa} \sim 10^{-4}$. (Here the slopes at the surface are compared to mean values at depth, presuming that the slopes, unlike the offsets, are representative of deeper rock behavior.) Seeing comparable values at scales on the order of kilometers to tens of kilometers indicates yet a further invariance of earthquakes, with constant stress drop scaling holding not only at the scale of events, but at length scales far below the event scale within events.

Distribution of Slip Differences

Earlier we saw that for a variety of average measures of differences in slip at different separations, the ratios seemed to

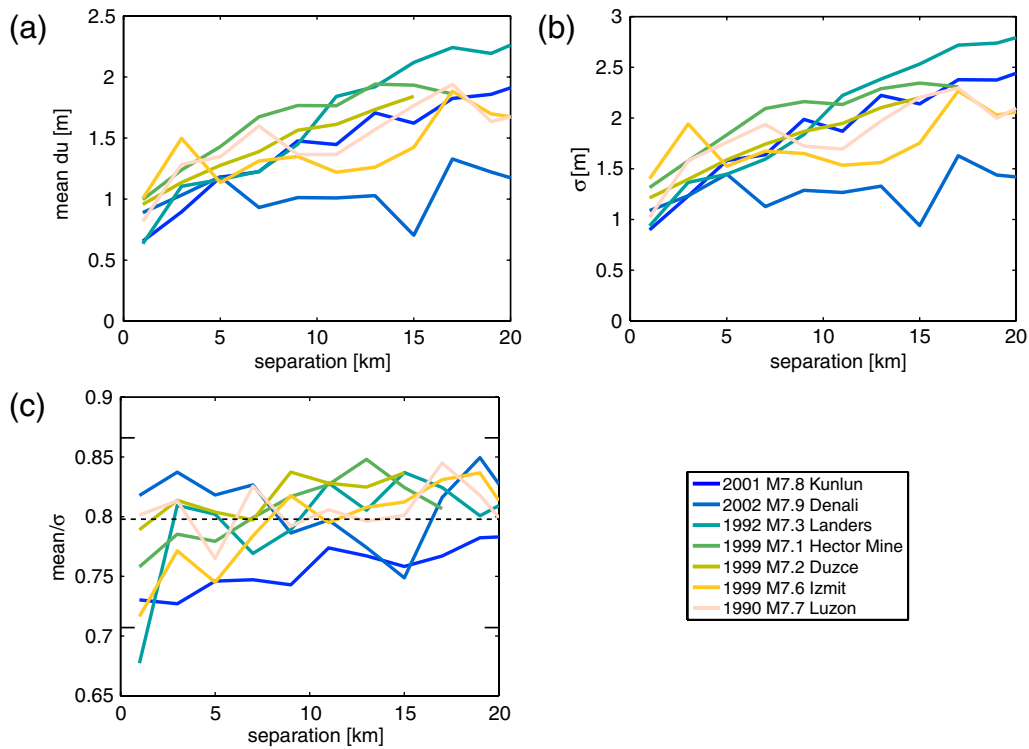


Figure 3. Averaging over slip differences as a function of separation. The different shades of curves are for each different earthquake, with the legend indicating which one. (a) Mean. (b) Standard deviation. (c) Mean/standard deviation. Averaging done only out to a maximum separation distance, which is 5 km less than half of the event length, to avoid finite size effects; thus, the two shortest events truncate before 20 km. The color version of this figure is available only in the electronic edition.

be well fit by values expected if the underlying distributions were normal. How well do normal distributions fit not just the low-order averages but also the full underlying distributions? A Lillie test shows that a quarter of the 70 distributions (10 bins times seven events) are rejected at the 5% confidence limit as being generated by a normal distribution. This factor of 5 enhanced rejection rate indicates that a normal distribution is not a perfect fit, but the 75% pass rate also indicates that it is not a bad fit either. Given that there are some differences, we would like to know in what ways the distributions differ from normal distributions. Are the differences in the tails, or are they somewhere else? Before, we looked at ratios of

low-order moments of the distributions, specifically in Figure 3c, the ratio of the first moment and the square root of the second moment. Generalizing this approach, we can look at the ratios of higher- and lower-order moments to probe the larger or smaller values. Defining

$$\Lambda_\eta \equiv \frac{[\int y^\eta p(y) dy]^{1/\eta}}{\int y p(y) dy}, \quad (2)$$

I plot this ratio of the moments as a function of the exponent η . To orient what we are looking at, with this ratio, Λ_η will be larger than for a normal distribution when $\eta > 1$ if the

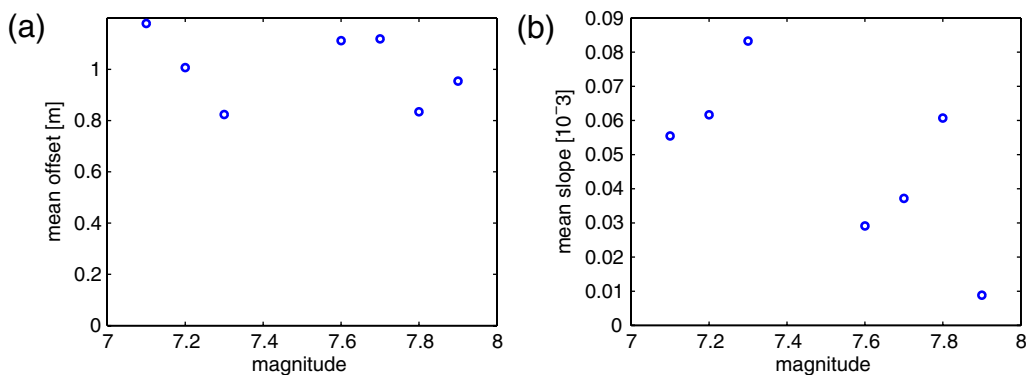


Figure 4. Linear fit to mean slip difference versus separation from Figure 3a. (a) Zero offset versus magnitude of the event. (b) Slope versus magnitude of the event. The color version of this figure is available only in the electronic edition.

distribution of observations has a heavier tail (more extreme values) than the normal distribution predicts. Figure 5 shows this plot for each of the bins in all the events, shading the bins by the separation (the darkest is close in, the lightest is farther away). Right away, two things can be seen. First, relative to a normal distribution (the thick dashed black line), there is a slight bias below the line at large η , more towards the boxcar function minimal tail (lower black dotted line) than the exponential function heavier tail (upper black dotted line). Thus, relative to a normal distribution, there is, slightly, an even sharper cutoff in the tails at the more extreme values. Second, there is a distance dependence to the bias, with closer separations having heavier tails than farther separations, the darkest curves tending to be slightly above the lightest ones at large η . These deviations can be interpreted as a consequence of having an absolute cutoff in what the differences can be, given by the maximum slip. This maximum slip cuts off the tails at higher separations, and, when present at shorter separations, contributes to heavier tails than a normal distribution of fluctuations would suggest.

Further details of the distributions of individual events affirm what has been seen in these averages of moments. Figure 6 shows how each of the bins' distributions deviate from what one would expect from a normal distribution, illustrated by plotting the cumulative distribution of differences with a nonlinear axis. (Here, unlike equation (1), $i \neq j$ is considered, and the sign of the difference in slip

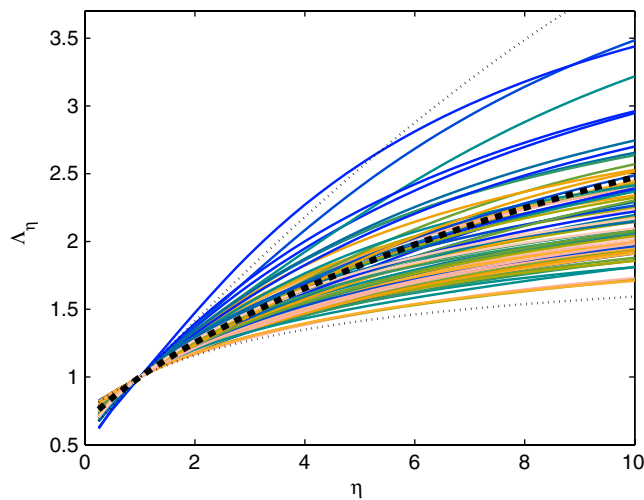


Figure 5. Ratio of moments to mean, as in equation (2). Shading is for different separation bins, with the darker shades being the closest and the lighter shades being the farthest. Results for all seven large earthquakes are superposed. The central thick dashed line shows the curve corresponding to a normal distribution. The top dotted line shows the curve corresponding to a heavier tailed exponential distribution. The bottom dotted line shows the curve corresponding to a lighter tailed boxcar function distribution. Note the slight progression from heavier tails to lighter tails for increasing separation, indicated by the darker curves tending to lie above the lighter curves. This is consistent with a slight upward trend in the ratio of the mean to the standard deviation shown in Figure 3c. The color version of this figure is available only in the electronic edition.

is included, giving an overall antisymmetric shape to the curves, to best view any deviation from normal distributions.) Curvature towards the vertical on these plots indicates lighter tails than a normal distribution, while curvature towards the horizontal indicates heavier tails. The slight tendency to curvature towards the vertical is evident in these plots.

All this focus on deviations from normal distribution behavior should not distract one from a central point, illustrated well by Figure 3: the average behavior is well fit by the average behavior of normal distributions. To the extent that small deviations from normal distribution behavior are found, the small deviations are found in the tails, with biases towards tails which fall off even more steeply than normal distributions, and this effect becomes more pronounced at larger separations.

Modeling the Behavior

To confirm understandings of the measurements and the constraints they place, I examine the results of applying the data analysis techniques to synthetic slip data. The first test is to apply uncorrelated random slip noise to the real data to show that the results are not sensitive to noise in the data and also to show that the input noise maps correctly onto the offset as expected. Figure 7 shows the ensemble for added slip ΔS chosen as the absolute values of normally distributed random slip with standard deviation ξ , with $\xi = 0, 1,$ and 2 m, respectively, in the panels. Robust behavior for added noise is seen, and it is mapping onto the offset, as expected.

How do synthetic slip functions compare with the data? Figure 8 shows various input slip functions. Figure 8a shows the results of the real data, for comparison with the synthetic distributions that follow. Figure 8b shows a triangle. Figure 8c shows a square root of sine function, based on a fit of stacked average slip data (Biasi and Weldon, 2006). Figure 8d shows a stepped increase in slip, based on a model of the Denali event (Haeussler *et al.*, 2004). Figure 8e shows a spectrally rough model, using a power law spectrally weighted k^{-p} with $p = 2.2$ (Helmstetter and Shaw, 2006). Figure 8f shows a modified Wiener process model (cumulative normally distributed noise detrended and absolute value so it is nonnegative everywhere). All contain, in addition to these correlated slip functions, an additional amount of uncorrelated slip noise. Using the same fitting procedure as was done with the real data, the average, standard deviation, and ratio of the standard deviation to the average are plotted.

By studying different noise amplitudes and different underlying slip distribution amplitudes, one learns that the amplitude of the noise at small separations and the average slip gradients at seismogenic depth scale separations together combine to create the dominant signal. Unfortunately, smaller scale features seem swamped by the noise. Thus, the measures studied have some discriminating power but, not surprisingly, not complete discriminating power.

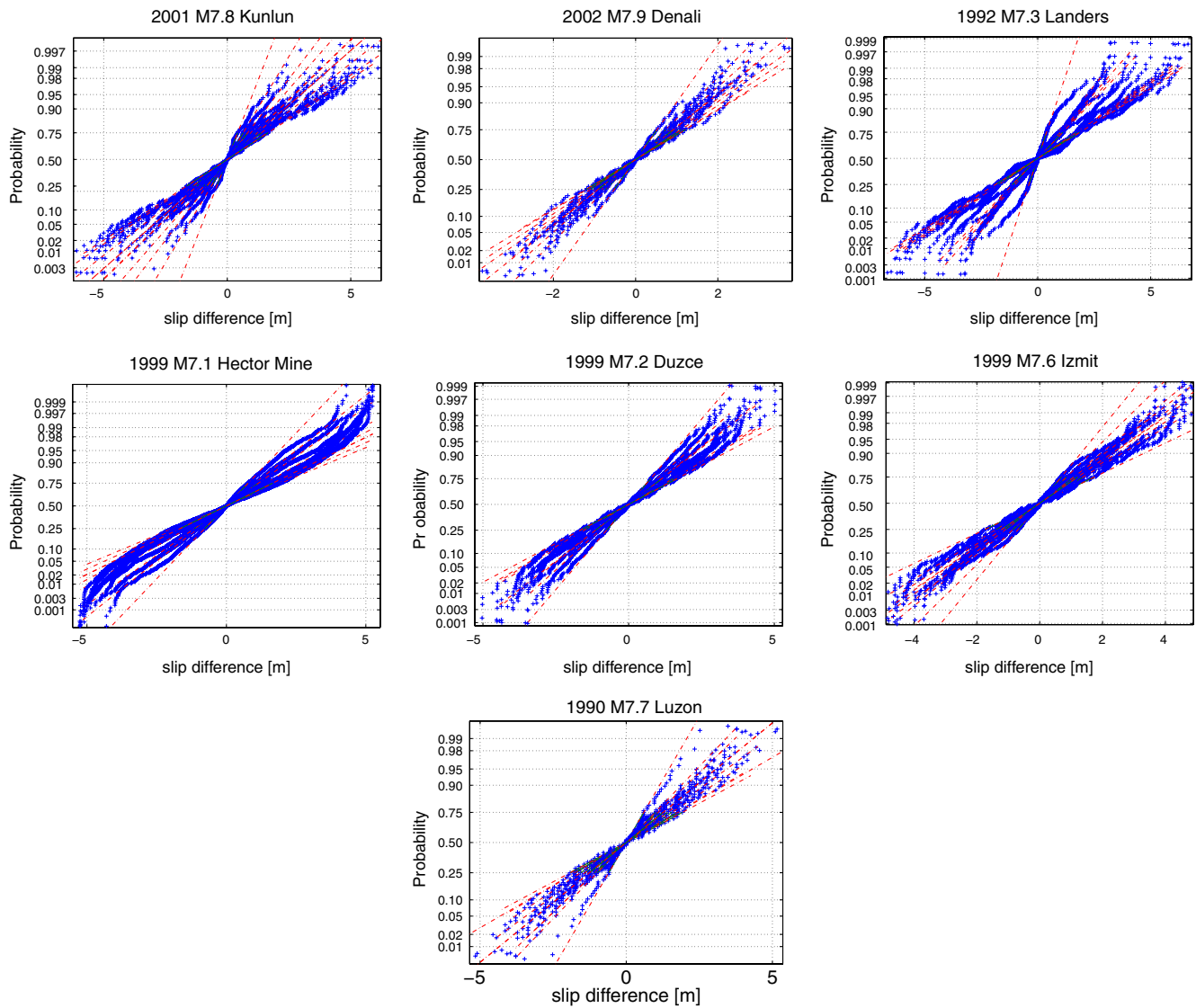


Figure 6. Cumulative pdf fit of normal distribution to the sets of data in each 2 km bin. The general lack of curvature in the vast majority of the curves indicates that a normal distribution is generally a good fit to the data. Dashed lines show linear fit to each bin. The slight curvature towards the vertical, as opposed to the horizontal, indicates that the slight deviations from normal distributions that do exist tend to have lighter tails (less extreme values) than normal distributions (as opposed to heavier tails indicated by curvature towards the horizontal). The color version of this figure is available only in the electronic edition.

The small mean slope seen in Denali can be reproduced by the two models, the stepping model in Figure 8d and the square root of sine in Figure 8c, where increases are concentrated over narrow regions, and typical differences are not changing much with separation. The other models with larger coherent changes on seismogenic crust depth scales and below better fit the other moderate mean slope events, so having more broadly distributed changes in slip rather than just concentrated changes in slip best fits most of the events. The triangle model, Figure 8b, fails in fitting any of the event data well due to the poor fit of the slip differences at larger separations to a normal distribution, evidenced by the too-fast growth in the mean-to-standard-deviation ratio at large separations. Thus, the two models which best fit most of the events are the two variable slip models; the spectrally

rough model, Figure 8e; and the modified Wiener process model, Figure 8f.

The modeling shows that local behavior at the seismogenic crust depth scales and below are indeed mapping onto the signal seen at these scales. The modeling affirms that noise is a substantial part, but certainly not all, of the signal. Noise alone would give a flat curve with no upward trend, which is obviously inconsistent with the data. On the other hand, ignoring the noise leads to obvious inconsistencies at zero separation with insufficient offset there. Thus, the data consist of noise and some underlying signal. My analysis helps to quantify aspects of both of these features. As Figure 8 illustrates, a noise of around $\xi = 1.25$ m, having a mean offset of around 1 m, gives a good fit of the synthetic data to the observations.

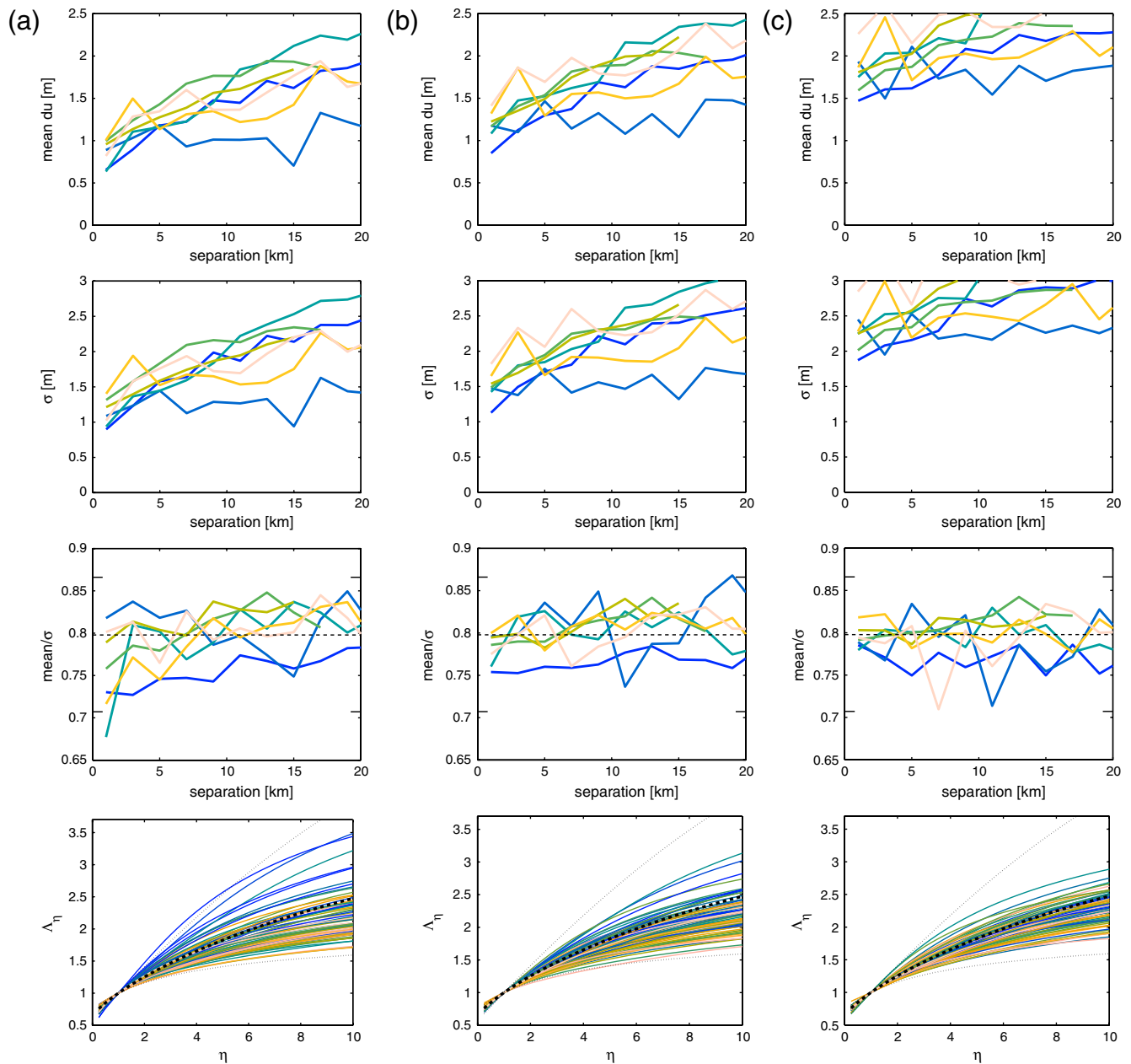


Figure 7. Robustness of measures with respect to adding noise to the real data, showing that added noise is mapping onto measures as expected. Rows from top to bottom are shown mean, standard deviation, ratio of mean to standard deviation, and moments of distribution. Columns give different values of noise added: (a) noise = 0, (b) noise = 1 m, and (c) noise = 2 m. The color version of this figure is available only in the electronic edition.

Coherent Structures

Having better understood the noisy environment of the measurements, I turn to an alternative way of looking at the data, seeking coherent structures that are unlikely to be noise dominated.

In an environment swamped by uncorrelated noise, slip increases are just as likely to be followed by slip decreases. Finding a long sequence of slip changes all of the same sign means that these are unlikely to be caused by noise. Indeed, for a sequence of n changes of the same sign, the probability

of it being caused by uncorrelated noise is 2^{-n+1} . Selecting sequences with $n \geq 5$, the vast majority of these will reflect underlying coherent processes (only 1/16 or less of the curves should have occurred by chance). The selection process will necessarily miss many if not most structures. The idea is that hopefully, the structures it does detect will be representative of some features of the underlying coherent processes. As will be seen, this hope appears to be realized.

Here, because what is being done is not a statistical analysis and because we are looking for potential magnitude dependence, the criteria used in the previous section are

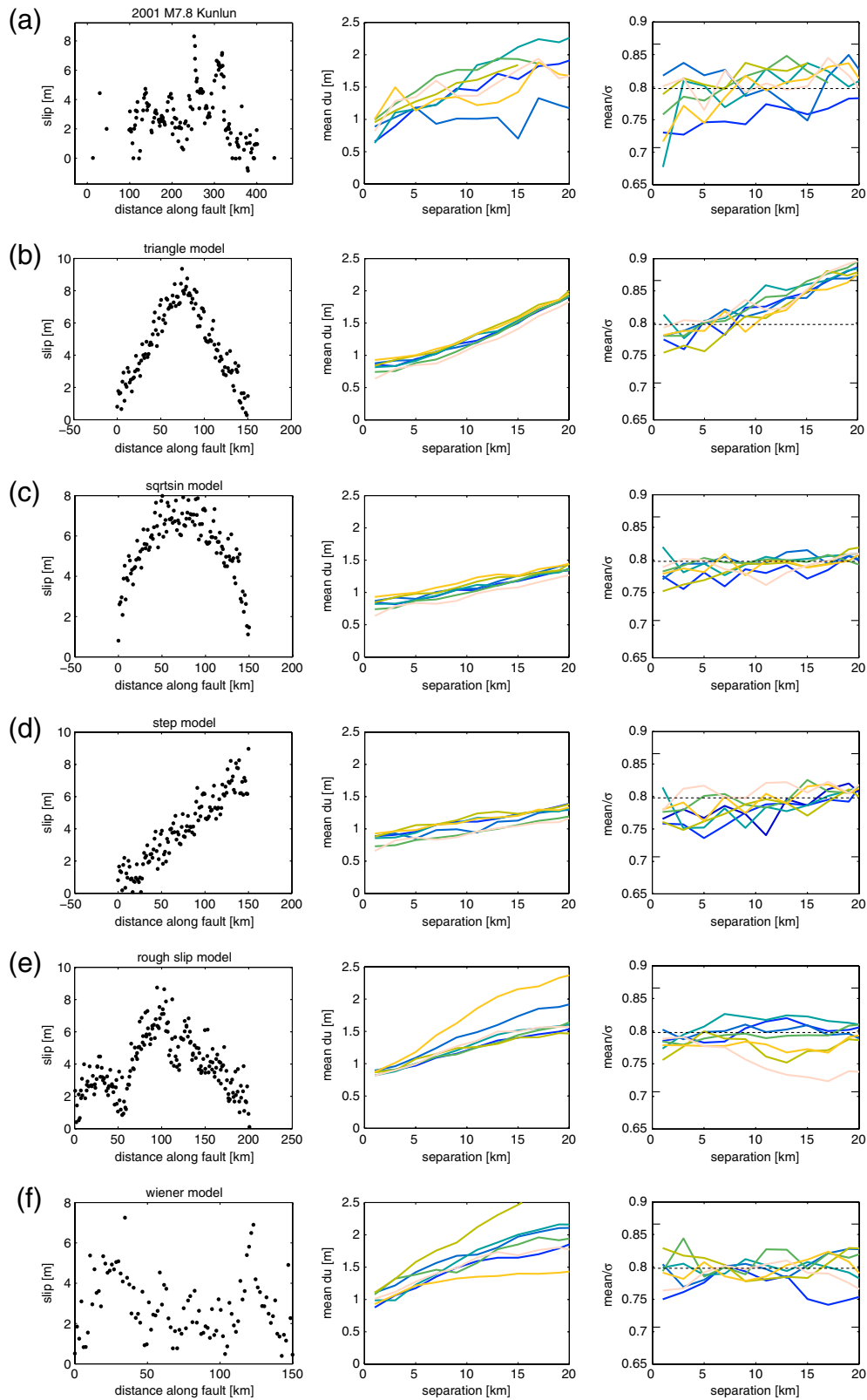


Figure 8. Comparison of real data with synthetic model slips. Synthetic slip functions include the uncorrelated slip noise component added to the base correlated slip. The uncorrelated noise has mean amplitude 1 m in the model cases shown. For each type of model slip, seven examples are calculated because that is the sample size for the real data, with one example from the seven plotted on the left to illustrate the type of slip distribution. (a) Real data, Kunlun example. (b) Triangular slip function. (c) Square root of sine function (see [Biasi and Weldon, 2006](#)). (d) Stepped increase (see [Haessler et al., 2004](#)). (e) Spectral power law (see [Helmstetter and Shaw, 2006](#)). (f) Modified Wiener process. The color version of this figure is available only in the electronic edition.

relaxed, and additional events from the database are included in the search. I searched for additional events from the database by dropping the magnitude and minimum number of slip measurement requirements. This led to a dozen extra events being searched. From the approximately 20 events searched in the database, 13 coherent structures were found from seven different events (the events in which structures were found were 2001 M 7.8 Kunlun, 1992 M 7.3 Landers, 1999 M 7.2 Duzce, 1954 M 6.8 Dixie Valley, 1988 M 6.6 Tennant Creek, 1968 M 6.5 Borrego Mountain, 1986 M 5.9 Marryat Creek). Figure 9 shows events not already shown in Figure 1 that were found to have coherent structures (sequences of slip values meeting the criteria of being sequentially increasing or sequentially decreasing for $n \geq 5$ points, highlighted in Figures 1 and 9 with lighter shade). Of the additional events in which coherent structures were found that were not previously analyzed, shown in Figure 9, three of the four are thrust and normal faulting events (Dixie Valley, normal; Tennant Creek and Marryat Creek, thrust), unlike the exclusively strike-slip events considered in Figure 1. In the case of Tennant Creek and Marryat Creek, the data are for vertical scarp height, which is not the same as

net surface slip on dipping faults. To compare these two cases against the others in terms of slip and slip gradients, the dip of the faults (45° for Tennant Creek, 35° for Marryat Creek) is accounted for, with the scarp height values multiplied by the inverse sine of these angles to get downdip slip and the corrected downdip slip values used in the figures that follow, which combine the different events. Extending the analysis to these other types of events helps to extend the magnitude range over which scaling effects can be looked for. As will be seen, they do not appear to show obvious differences with the large strike-slip events from Figure 1 in terms of coherent structures. Thus, they are included in the analysis that follows. Regarding the representativeness of the coherent structures that are detected by the criteria specified, looking at the plots, the highlighted stretches do not seem particularly special and by eye, seem to represent typical behaviors of high sloping regions in other areas, which happen not to have long sequential stretches.

Figure 10 shows, superposed on common axes, the coherent structures found. Examining the plot, I find that the relatively low scatter of the slip around average slope profiles indicates that the procedure is picking up mostly

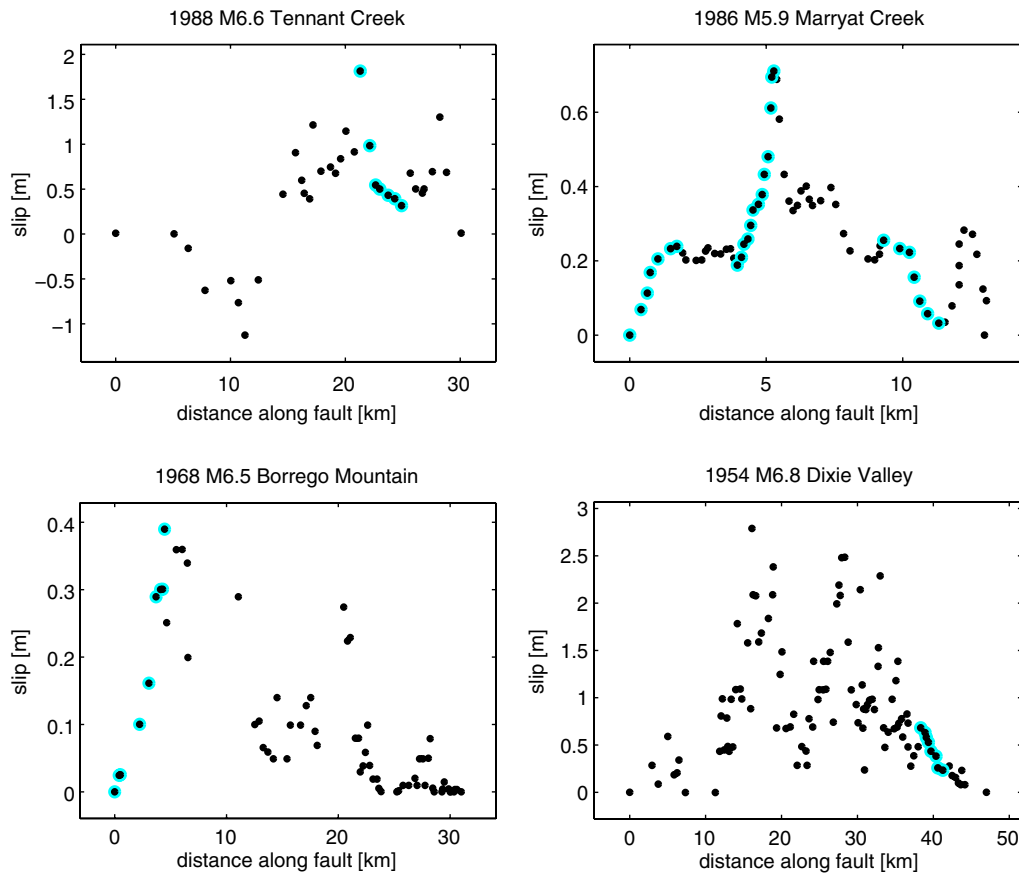


Figure 9. Surface-slip data for earthquakes that have coherent structures and are not already shown in Figure 1. Coherent structures are defined as having at least $n \geq 5$ consecutive increasing or consecutive decreasing slip values. The coherent structures are highlighted in a lighter shade. Original sources for the earthquakes shown here (from the Wesnousky [2008] data set) are as follows: 1988 M 6.6 Tennant Creek (Crone *et al.*, 1992); 1986 M 5.9 Marryat Creek (Machette *et al.*, 1993); 1968 M 6.5 Borrego Mountain (Clark, 1972); 1954 M 6.8 Dixie Valley (Caskey *et al.*, 1996). The color version of this figure is available only in the electronic edition.

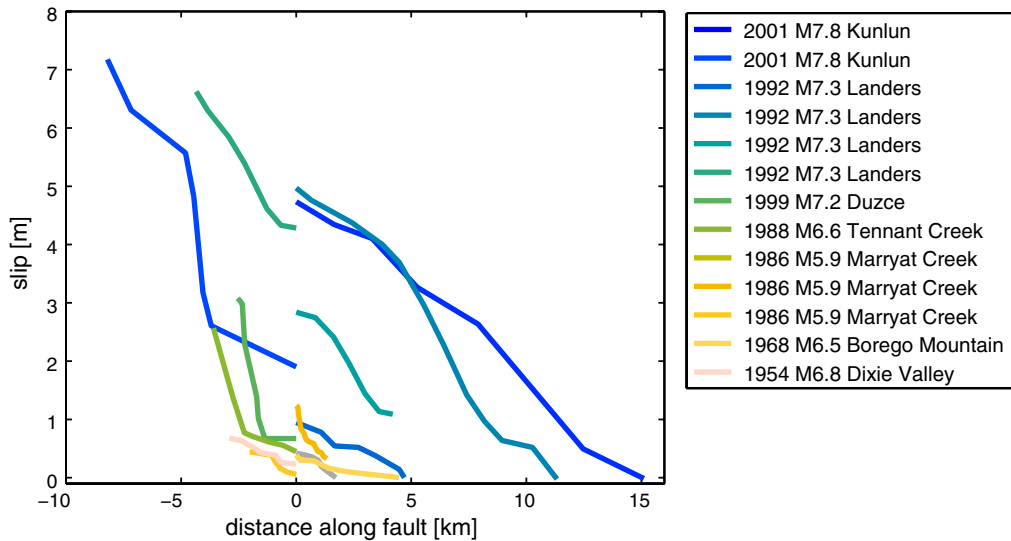


Figure 10. Slip versus distance along fault for coherent structures extracted by requiring n adjacent points to all have slip increments of the same sign, either all increasing or all decreasing. For visualization purposes, the increasing points are shown as decreasing to the left of the zero relative distance along the fault. Note the relatively low scatter for each line around the average slopes, indicating signals are above the noise levels in these structures. Here, $n \geq 5$ is used. Line shading helps to show different profiles; some events have multiple structures. The color version of this figure is available only in the electronic edition.

coherent signals. As a further test that the analysis is indeed picking up relevant structures and not just statistical noise, I repeated the measurements for the case where a large-amplitude uncorrelated noise was added to all the slip measurements. An ensemble of noise measurements showed that on average only around one structure was found in these uncorrelated noise dominated cases, in contrast with the 13 structures found here. Thus, the great majority of the detected structures are indeed not just noise.

Figure 11 shows fits to the slip gradients as a function of two features of the slip structures: in Figure 11a, scale length over which the structure occurred and in Figure 11b, magnitude of the event the coherent structure. In both cases, importantly, there is a lack of any obvious trend. That is, coherent surface-slip strain values appear to be independent of length scale and also independent of event magnitude.

The strain values seen are, interestingly, not very big. They are significantly larger than the average lateral strain values seen in the previous analysis, but that is not surprising given that we are selecting for regions which stand out above the noise in the system. Interestingly, they are about a factor of 10 larger than the average behavior found in the statistical analysis but remain modest in terms of absolute value: earthquakes generally appear not to change their underlying slip very suddenly.

Conclusions

I have developed a new way of statistically analyzing surface-slip measurements to examine surface-slip gradients in large earthquakes. A good collapse of the data is found, with scatter around the median of less than a factor of 2 and

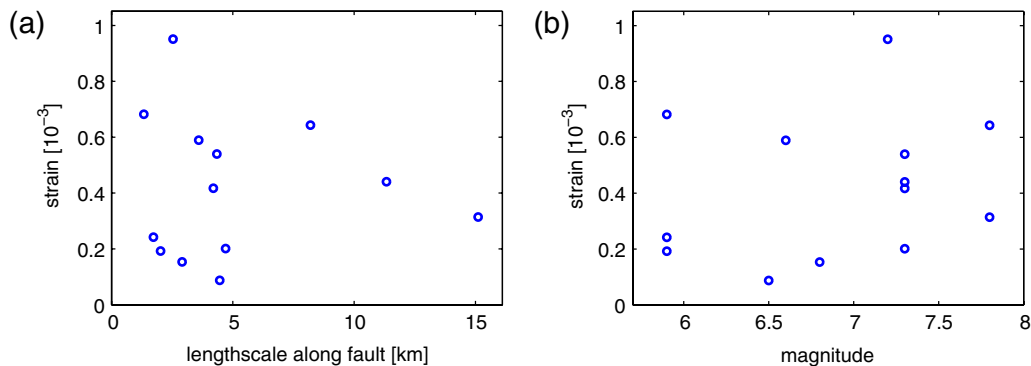


Figure 11. Slip gradients in coherent structures fit to data in Figure 10. (a) Gradients as a function of length of the coherent structure. (b) Gradients as a function of magnitude of the event producing the coherent structure. From (b) we see that seven different events in the data set have sections of slip that meet the criteria and are contributing data points to the plots; some events, such as Landers, contribute multiple data points. Note in both plots the lack of a clear trend in the data, indicating possible length-scale and magnitude independence of the surface-slip gradients. The color version of this figure is available only in the electronic edition.

common behavior over kilometer to tens-of-kilometer length scales, suggesting that this is a useful projection of the data.

I have found distributions of differences of slip to be reasonably well fit by normal distributions, with the standard deviation in the normal distributions growing linearly with distance. Mean measurement differences trend consistently to an offset extrapolated back to zero separation of around 1 m. A fundamental open question is to ask what the source of this zero-separation offset is. Is it measurement noise, effects of the near-surface nonlinear unconsolidated sediment behavior, nonplanar geometry effects, interesting source effects? This analysis does not answer these questions, but it is hoped that the work quantifying this noise term stimulates further progress on these questions. Fortunately, the future holds further promise in getting at these issues through hugely improved data. Specifically, the B4 LiDAR (light detection and ranging) mapping of faults (Hudnut *et al.*, 2002), when combined with a future B5 picture after large surface rupturing events, should produce unprecedented density and accuracy of slip data. Such data, when analyzed in the manner outlined in this paper, should help tremendously in identifying the sources of, and perhaps reducing significantly, the variability in slip. Extending this analysis to such a data set would be tremendously exciting.

Developing a better understanding of the noise inherent in the signals has enabled the extraction of interesting measures of the underlying signal. Subtracting the zero offset, average lateral surface strains at kilometer to tens-of-kilometer length scales were found to be comparable to average strain drops at the event scale. This extends previous observations of constant stress drop scaling at the scale of events across populations of events at very different length scales (Aki, 1972; Hanks, 1977; Shaw, 2009) into a whole new regime, with now-constant stress drop scaling observed within events at length scales smaller than the event scale, revealing a further symmetry of earthquake dynamics.

Analyzing the data beyond statistical measures but remaining cognizant of the noise, I looked for coherent structures in the slip gradients. By examining long sequences of increasing or sequences of decreasing measurements unlikely to be caused by noise, a set of slip gradients were found in the surface data. These coherent structures were found to have moderate strain values, not surprisingly larger than average values (they were, after all, selected to stand out above the noise). The values found, on the order of a factor 10 times the average measurements, were interesting in a number of ways. First, they were not all that large, suggesting earthquakes generally do not change their underlying slip very suddenly. Second, neither a length scale nor a magnitude dependence was seen in the values, indicating potential scale invariant behavior in the coherent structures.

Looking ahead, these statistical and coherent structure analyses of surface-slip data would all benefit from denser measurement, and better quantifications of uncertainties in the measurements. This is a tremendously important window into earthquake source behavior, and there is no doubt

more to be learned from analyzing these sub-event-scale observations. I eagerly await a B4–B5 event.

Data and Resources

Slip data are taken from an extensive list of primary data compiled by Wesnousky (2008) from a wide range of sources and included in the electronic supplement to that paper. References to the original sources of data are listed in the captions of Figures 1 and 9.

Acknowledgments

I thank Yuri Fialko for useful discussions. I thank Glenn Biasi and an anonymous reviewer for constructive comments. I also thank Biasi for suggesting that potential biases in the data collection might be one potential source of the nonzero slip difference offset at small separations. This work was supported by NSF EAR-0911221, EAR-0934736, and EAR-0943939 and by the Southern California Earthquake Center (SCEC).

References

- Aki, K. (1972). Earthquake mechanism, *Tectonophysics* **13**, 423–446.
- Akyuz, H., R. Hartleb, A. Barka, E. Altunel, G. Sunal, B. Meyer, and R. Armijo (2002). Surface rupture and slip distribution of the 12 November 1999 Duzce earthquake (M 7.1), North Anatolian fault, Bolu, Turkey, *Bull. Seismol. Soc. Am.* **92**, 1, 61–66.
- Barka, A., H. Akyuz, E. Altunel, G. Sunal, Z. Cakir, A. Dikbas, B. Yerli, R. Armijo, B. Meyer, J. de Chabaliere, T. Rockwell, J. Dolan, R. Hartleb, T. Dawson, S. Christofferson, A. Tucker, T. Fumal, R. Langridge, H. Stenner, W. Lettis, J. Bachhuber, and W. Page (2002). The surface rupture and slip distribution of the 17 August 1999 Izmit earthquake (M 7.4), North Anatolian fault, *Bull. Seismol. Soc. Am.* **92**, no. 1, 43–60.
- Biasi, G. P., and R. J. Weldon (2006). Estimating surface rupture length and magnitude of paleoearthquakes from point measurements of rupture displacement, *Bull. Seismol. Soc. Am.* **96**, 1612–1623, doi [10.1785/0120040172](https://doi.org/10.1785/0120040172).
- Bodin, P., and J. N. Brune (1996). On the scaling of slip with rupture length for shallow strike-slip earthquakes: Quasistatic models and dynamic rupture propagation, *Bull. Seismol. Soc. Am.* **86**, 1292–1299.
- Caskey, S., S. Wesnousky, P. Zhang, and D. Slemmons (1996). Surface faulting of the 1954 Fairview Peak (M_s , 7.2) and Dixie Valley (M_s , 6.8) earthquakes, central Nevada, *Bull. Seismol. Soc. Am.* **86**, no. 3, 761–787.
- Clark, M. M. (1972). Surface rupture along the Coyote Creek fault, the Borrego Mountain Earthquake of April 9, 1968, *U.S. Geol. Surv. Profess. Pap.* **787**, 55–86.
- Crone, A. J., M. N. Machette, and R. J. Bowman (1992). Geologic investigations of the 1988 Tennant Creek, Australia, earthquakes—implications for paleoseismicity in stable continental regions, *U.S. Geol. Surv. Bull.* **2032-A**, 51 pp.
- Haeussler, P., D. Schwartz, T. Dawson, H. Stenner, J. Lienkaemper, B. Sherrod, F. Cinti, P. Montone, P. Craw, A. Crone, and S. Personius (2004). Surface rupture and slip distribution of the Denali and Totschunda faults in the 3 November 2002 M 7.9 earthquake, Alaska, *Bull. Seismol. Soc. Am.* **94**, 6B, S23–S52.
- Hanks, T. C. (1977). Earthquake stress-drops, ambient tectonic stresses, and the stresses that drive plates, *Pure Appl. Geophys.* **115**, 441–458.
- Helmstetter, A., and B. E. Shaw (2006). Estimating stress heterogeneity from aftershock rate, *J. Geophys. Res.* **111**, B07, 304, doi [10.1029/2005JB0040077](https://doi.org/10.1029/2005JB0040077).
- Hemphill-Haley, M. A., and R. J. Weldon (1999). Estimating prehistoric earthquake magnitude from point measurements of surface rupture, *Bull. Seismol. Soc. Am.* **89**, 1264–1279.

- Hudnut, K. W., A. Borsa, C. Glennie, and J. B. Minster (2002). High-resolution topography along surface rupture of the 16 October 1999 Hector Mine, California, earthquake (M_w 7.1) from airborne laser swath mapping, *Bull. Seismol. Soc. Am.* **92**, 1570–1576.
- Klinger, Y., X. W. Xu, P. Tapponnier, J. Van der Woerd, C. Lasserre, and G. King (2005). High-resolution satellite imagery mapping of the surface rupture and slip distribution of the M_w 7.8, 14 November 2001 Kokoxili earthquake, Kunlun Fault, Northern Tibet, China, *Bull. Seismol. Soc. Am.* **95**, 1970–1987.
- Klinger, Y., R. Michel, and G. King (2006). Evidence for an earthquake barrier model from M_w similar to 7.8 Kokoxili (Tibet) earthquake slip-distribution, *Earth Planet. Sci. Lett.* **242**, 3–4, 354–364, doi [10.1016/j.epsl.2005.12.003](https://doi.org/10.1016/j.epsl.2005.12.003).
- Lin, A., B. Fu, J. Guo, Q. Zeng, G. Dang, W. He, and Y. Zhao (2002). Co-seismic strike-slip and rupture length produced by the 2001 M_s 8.1 Central Kunlun earthquake, *Science* **296**, 5575, 2015–2017.
- Machette, M. N., A. J. Crone, and J. R. Bowman (1993). Geologic investigations of the 1986 Marryat Creek, Australia, earthquake—implications for paleoseismicity in stable continental regions, *U.S. Geol. Surv. Bull.*, 2032-B, 29 pp.
- Manighetti, I., M. Campillo, C. Sammis, P. M. Mai, and G. C. P. King (2005). Evidence for self-similar, triangular slip distributions on earthquakes: Implications for earthquake and fault mechanics, *J. Geophys. Res.* **110**, B05302, doi [10.1029/2004JB003174](https://doi.org/10.1029/2004JB003174).
- Manighetti, I., M. Campillo, S. Bouley, and F. Cotton (2007). Earthquake scaling, fault segmentation, and structural maturity, *Earth Planet. Sci. Lett.* **253**, 429–438.
- Nakata, T. (1990). Surface faulting associated with the Philippine earthquake of 1990, *J. Geogr.* **99**, 95–112.
- Rockwell, T. K., S. Lindvall, T. Dawson, R. Langridge, W. Lettis, and Y. Klinger (2002). Lateral offsets on surveyed cultural features resulting from the 1999 Izmit and Duzce earthquakes, Turkey, *Bull. Seismol. Soc. Am.* **92**, 79–94.
- Romanowicz, B. (1992). Strike-slip earthquakes on quasi-vertical transcurrent fault: inferences for general scaling relations, *Geophys. Res. Lett.* **19**, 481–484.
- Romanowicz, B. (1994). Comment on 'A reappraisal of large earthquake scaling' by C. Scholz, *Bull. Seismol. Soc. Am.* **84**, 1675–1676.
- Scholz, C. H. (1982). Scaling laws for large earthquakes: consequences for physical models, *Bull. Seismol. Soc. Am.* **72**, 1–14.
- Scholz, C. H. (1994). Reply to comments on 'A reappraisal of large earthquake scaling', *Bull. Seismol. Soc. Am.* **84**, 1677–1678.
- Shaw, B. E. (2009). Constant stress drop from small to great earthquakes in magnitude-area scaling, *Bull. Seismol. Soc. Am.* **99**, 871–875, doi [10.1785/0120080006](https://doi.org/10.1785/0120080006).
- Shaw, B. E., and C. H. Scholz (2001). Slip-length scaling in large earthquakes: Observations and theory and implications for earthquake physics, *Geophys. Res. Lett.* **28**, 2995–2998.
- Sieh, K., L. Jones, E. Hauksson, K. Hudnut, D. Eberhart-Phillips, T. Heaton, S. Hough, K. Hutton, H. Kanamori, A. Lilje, S. Lindvall, S. F. McGill, J. Mori, C. Rubin, J. A. Spotila, J. Stock, H. K. Thio, J. Treiman, B. Wernicke, and J. Zachariasen (1993). Near-field investigations of the Landers earthquake sequence, April to July 1992, *Science* **260**, 5105, 171–176.
- Treiman, J., K. Kendrick, W. Bryant, T. Rockwell, and S. McGill (2002). Primary surface rupture associated with the M_w 7.1 16 October 1999 Hector Mine earthquake, San Bernardino County, California, *Bull. Seismol. Soc. Am.* **92**, 4, 1171–1191.
- Wells, D. L., and K. J. Coppersmith (1994). New empirical relationships among magnitude, rupture length, rupture width, rupture area, and surface displacement, *Bull. Seismol. Soc. Am.* **84**, 974–1002.
- Wesnousky, S. G. (2008). Displacement and geometrical characteristics of earthquake surface ruptures: Issues and implications for seismic-hazard analysis and the process of earthquake rupture, *Bull. Seismol. Soc. Am.* **98**, 1609–1632.
- Xu, X., W. Chen, W. Ma, G. Yu, and G. Chen (2002). Surface rupture of the Kunlunshan earthquake (M_s 8.1), northern Tibetan plateau, China, *Seism. Res. Lett.* **73**, 884–892.
- Yomogida, K., and T. Nakata (1994). Large slip velocity of the surface ruptures associated with the 1990 Luzon earthquake, *Geophys. Res. Lett.* **21**, 1799–1802.

Lamont Doherty Earth Observatory
Columbia University

Manuscript received 9 March 2010